

Measurements of the Radiation Belts from *Mir* and *STRV* 1994-1997

P. Buehler, A. Zehnder, L. Desorgher, W. Hajdas, Paul Scherrer Institute, CH-5232 PSI Switzerland

E. Daly, L. Adams, ESA/ESTEC, NL-2200-AG Noordwijk, The Netherlands

Abstract

Simple environment monitors were launched in 1994; one was placed in geostationary transfer orbit (GTO) onboard *STRV-1b* while the second was installed externally on *Mir* in LEO. GTO covers the equatorial regime of inner and outer radiation belts well. *Mir* encounters the belts near atmospheric cut-off. We summarize these observations. The outer (electron) belt has been subject to many injection events, including January 1997. *Mir* data show the strong anisotropy in the low-altitude inner (proton) belt. Results are compared with models.

I. INTRODUCTION

High energy radiation belt particles are an increasing threat to spacecraft and their payloads. Single-event upsets in electronics, radiation background, component degradation, electrostatic charging and astronaut hazards are among the effects. The need for small radiation monitors is becoming clearer, both for better mapping of the environment, and as an on-board resource for operations' use and to aid future mission planning. The REMs on *STRV* and *Mir* are simple pairs of single shielded silicon diode detectors. Despite the problems of radiation species cross-contamination and discrimination difficulties inherent in such devices, they are cheaper and easier to construct and accommodate than more discriminating, uncontaminated instruments. The results presented here, from the REM instruments operating for almost 3 years in two very different orbits, show that highly valuable results can be derived if care is taken with calibration and simulation. These data, and those expected from follow-on monitors will be a valuable data resource for modelling the radiation belts and monitoring the magnetospheric environment while many sensitive missions are flying. These will include space-based astronomy, communications constellations, and the International Space Station. Current static models are inadequate for many contemporary mission and spacecraft design purposes [1].

II. INSTRUMENTS AND SPACECRAFT

REM registers, discriminates and counts the pulses of charge (corresponding to particle energy deposit, ΔE)

generated by particle impacts on the Si diode detectors [2]. The pulse-height discrimination is arranged to optimally respond to electrons, protons and heavy ions over 16 ΔE channels in each of the two independent detectors. This is shown schematically in Figure 1.

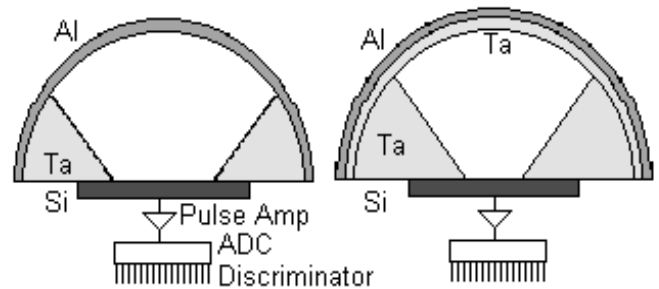


Figure 1: Schematic of a REM

A difficulty in building electron detectors is to prevent the counts from becoming contaminated by high energy protons. Electrons in the MeV range deposit close to the minimum ionizing energy in silicon (~ 0.37 keV/m) - about the same that protons with $E > 300$ MeV deposit. Therefore these particles cannot be unambiguously distinguished from ΔE measurements alone. This problem can be solved by using stacks of different detectors and active shielding, which complicates the system. In REM, we accept that electron channels can be contaminated by protons, but measure the proton flux independently to use this information to deduce the proton contribution in the electron channels. REM consists of two detectors in the arrangement shown in Fig.1. Each detector uses one silicon diode which is shielded by a spherical dome of 3 mm aluminium. One detector is shielded with an additional inner lining of $\frac{1}{2}$ mm tantalum which considerably lowers the penetration of MeV electrons, although they cannot be totally eliminated. (This we call the "p detector"; the other is the "e detector"). The e detector on *Mir* has a reduced shield of 0.7mm Al. By using the simultaneous measurements of both detectors, information on both electron and proton fluxes can be gained. The location also helps since the inner belt is proton-dominated and the outer belt consists of electrons most of the time. The e detector is sensitive to protons with energies $E > 30$ MeV and to electrons with energies $E > 1.2$ MeV

($>10\text{MeV}$ and $>0.7\text{MeV}$ respectively for *Mir*) while the p detector responds to protons above 40MeV . The energy transfer spectra are accumulated for typically 100 sec (32 sec. on *Mir*) and binned into 16 detector ΔE channels. The main aperture of the instrument is defined by a cone of 45° . Due to mass restrictions on *STRV* the surrounding shielding is not ideal and some very high energy protons can penetrate from the sides. On *Mir*, the bulk of the station provides considerable rear shielding. An important input for the spectral deconvolution of the measured ΔE histograms are the energy-dependent geometric factors. Special efforts have been taken to determine the geometric factors of the REM detectors. The flight instruments were calibrated with protons and electrons at various energies. In addition, they were extensively simulated numerically, through Monte-Carlo software, including realistic models of the mass distribution of the spacecraft. The UK micro-satellite *STRV-1b* is in a Geostationary Transfer Orbit, GTO, with 250 km perigee, 36000km apogee, a 7° inclination, and a $10\frac{1}{2}$ hr. period. GTO cuts through both inner (“proton”) and outer (electron) radiation belts. An EVA in late 1994 was used to fix another model to the outside of the Russian space station *Mir*, which orbits the earth in a circular Low Earth Orbit, LEO (400 km, 51.6° inclination, 90 min period).

Mir encounters inner belt protons in the south Atlantic anomaly and outer belt electrons at high latitudes.

III. SUMMARY OF OBSERVATIONS

A. GTO Radiation Belt Measurements

The influence of solar-heliospheric events on the radiation belts is a strong feature of the REM observations. The period covered by REM measurements corresponds to the declining phase of the 11-year solar activity cycle. In the absence of significant solar energetic particle events, the solar wind (SW) arriving at the earth is characterized by recurrent fast SW streams. We see recurrent radiation-belt effects due to the 27-day solar rotation period. Figure 2 shows ~ 1 MeV electron fluxes measured by REM on *STRV-1b* at $L=4.5$ as a function of time. The repeated large flux peaks in the top panel are associated with the occurrence of fast SW streams impinging on the earth's magnetosphere. The dashed vertical lines are spaced at 27-day intervals. The 27-day repetition of rapid energetic electron depletions and injections is clear. The differences between solstice and equinox periods can be attributed to variations in the effectiveness of SW-magnetosphere interaction.

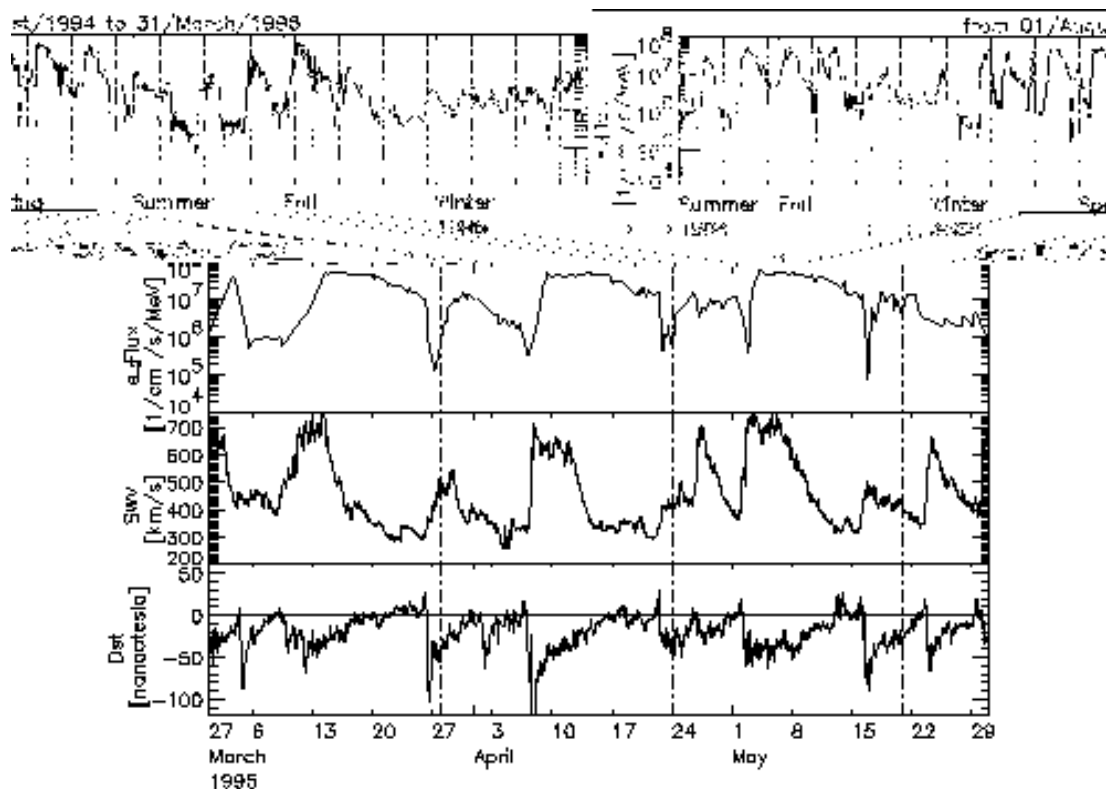


Figure 2: Electron belt flux variations measured by REM on *STRV* (see text for details).

The three lower panels show details of the spring 1995 period when there was a particularly strong series of recurrent interactions. The uppermost of the three shows the REM data, the second shows the SW speed as measured by the WIND spacecraft, and the lowest shows the D_{st} geo-magnetic index. The arrival of a fast SW stream at the earth first causes a depletion of the outer belt high energy electron population within about a day, followed by a rapid (~few days) increase where the flux level reached depends on the SW peak velocity. Fluxes then slowly decay. Figure 3 shows how the large electron injection of January 1997 which received wide media publicity [3] was seen by the REM on STRV. Each panel represents half an orbit (~5 hrs.), either the inbound or outbound passage. The period before this event was extremely quiet, with essentially no outer zone. The build-up by over 4 orders of magnitude in a matter of hour is clear. The transport of the belt is also seen, but care must be taken because of aliasing of time and space variations.

Figure 4 summarizes the orbital “dose” measurements, emphasizing the dynamicism of the electron environment. “Dose” in this context is the energy deposited in the detector excluding the lowest channel, so should not be confused with total ionizing dose.

Note that the January event of Fig. 3 was unexceptional in comparison to events in spring 1995. Also shown are the detector energy deposit predicted for this orbit by the static AE-8-MIN and AP-8-MIN models for the two detectors when fluxes are folded with the instrument response functions. P detector doses are not shown after July 1996 when the dead-time correction system became unusable.

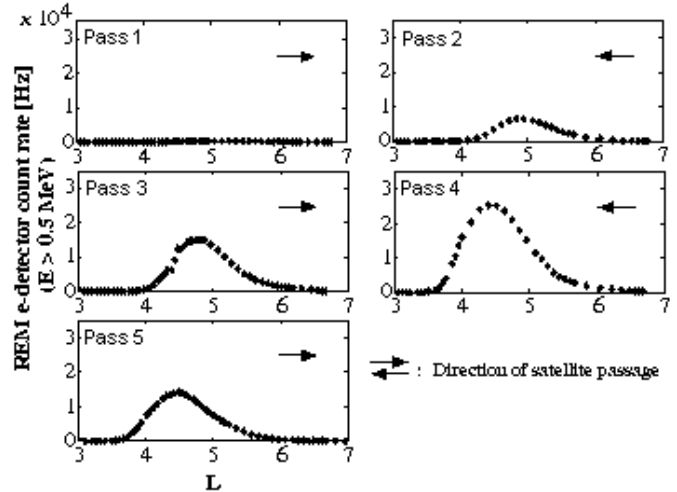


Figure 3: Injection Event of 10-11 January 1997

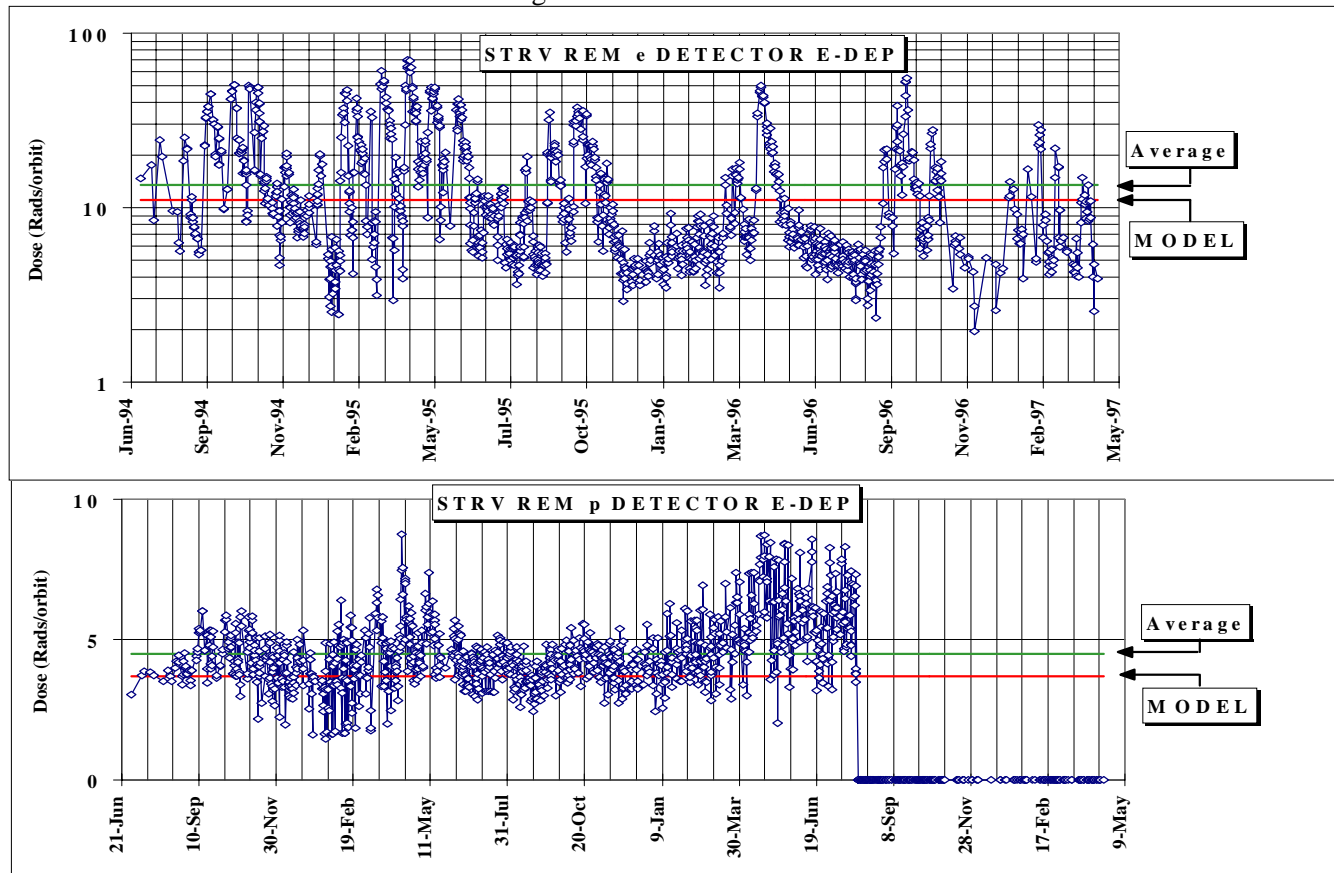


Figure 4: summary of STRV orbital dose rates in each detector, compared to model predictions

Both electron and proton models appear to underestimate dose, but only by a relatively small amount. Because of the dynamicism, the electron environment is not well represented by the model for long periods, even though on average the agreement is reasonable.

Apart from recurrent SW effects, we have observed that the energetic electron environment exhibits strong seasonal variations with peak activity occurring near equinoxes as shown in Fig. 5. This is a manifestation of magnetospheric-heliospheric connection geometry.

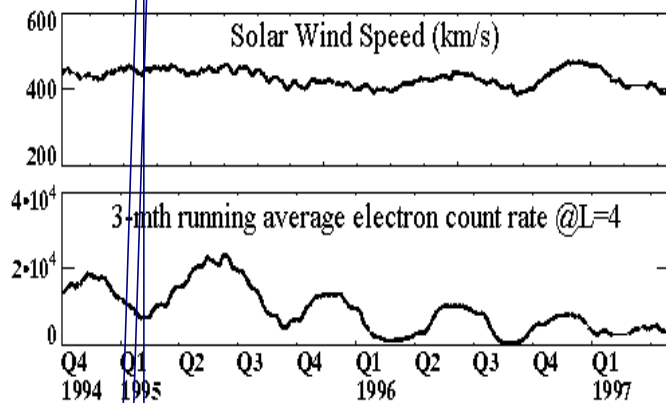
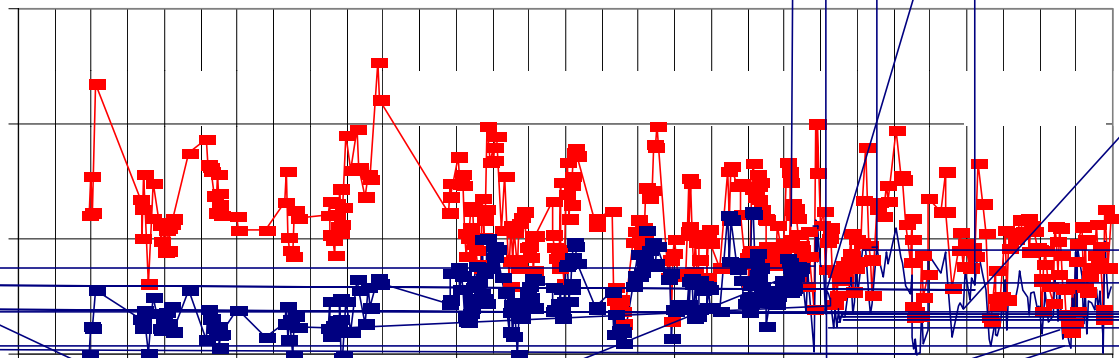


Figure 5: seasonal behavior of electrons >1.2 MeV

B. Mir Low Altitude Measurements

The radiation environment of *Mir* is dominated by inner belt protons. The largest proton fluxes are encountered at $L < 3$, in the South Atlantic anomaly. Figure 6 shows the dose summary for the two detector, separated into SAA ($L < 3$) and “polar” ($L > 3$) components. This shows that at $L > 3$, the electron dose is subject to the same dynamicism seen in the *STRV* data (note that the energy threshold is lower than on *STRV*), while the proton dose reflects the cosmic ray level. For $L < 3$, the variability is less, but a scatter is evident. This is partly due to real temporal variations, but is also due to anisotropy effects discussed below.

The proton dose shows an increasing trend as solar activity decreases while the electron dose appears to fall. The corresponding model predictions of dose are 112 and 0.25 mrad/day in e and p detectors respectively, for $L > 3$, and 72 and 70 mrad/day in e and p detectors respectively, for $L < 3$.



In Fig. 7 the daily average dose measured in the SAA by *Mir* REM is plotted together with the 3-month average $F_{10.7A}$ solar activity index, as functions of time. The $F_{10.7}$ index is also an indicator of upper atmosphere heating. Around the middle of 1995 the SAA dose increased by 25%. At the same time $F_{10.7A}$ decreased by about the same factor. Calculations show that the decrease in heating causes a lowering of atmospheric density in the SAA region by typically 20% which could be responsible for the enhanced SAA doses.

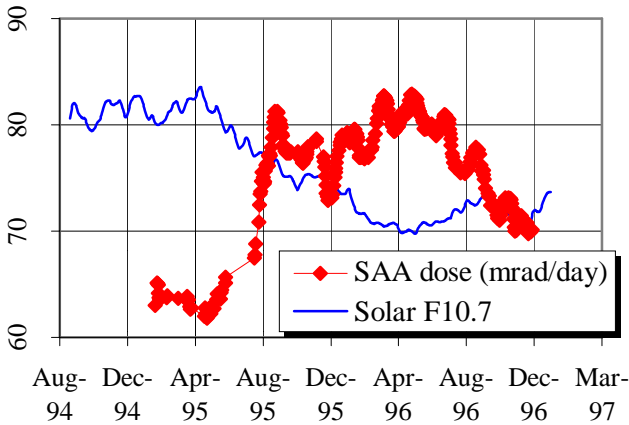


Figure 7: Average SAA proton doses and solar activity index

The atmosphere is also responsible for anisotropies in proton fluxes in the SAA. Large radius cyclotron motion of energetic protons in the SAA, where the dip angle is $\sim 50^\circ$, means that guiding centers of particles arriving from the east at a detector are below the point of observation, while for particles arriving from the west they are above. So particles from the east experience denser parts of the atmosphere than those from the west and will be more absorbed. The result is the “east-west” effect [4]. On *Mir*, REM is shielded from the back by the massive space station. So by sorting the observations by the orientation of the detectors with respect to the local magnetic field it was possible to measure the anisotropy [5]. Fig. 8 shows *Mir* REM count rates in the high energy proton channels at $L=1.4$ plotted as functions of B for different detector viewing directions. The average ratio between west and east is 4.3. Recently a model for the anisotropic proton flux has been included in ESA's radiation belt model software UNIRAD [6]. These present results are consistent with the model.

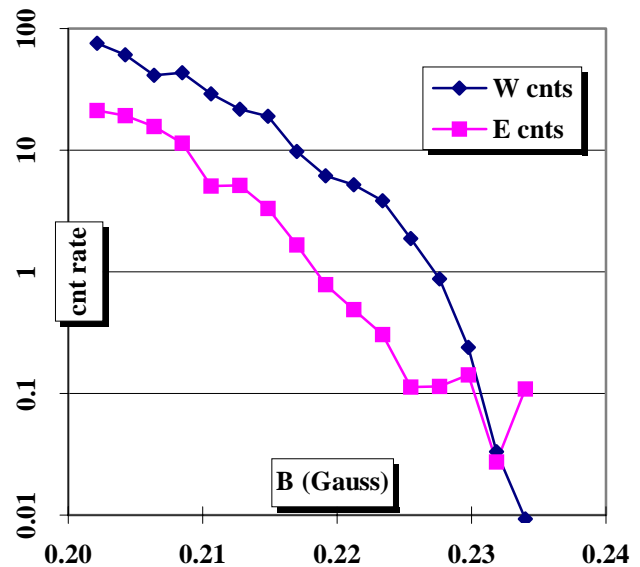


Figure 8: Anisotropy of SAA ($1.35 < L < 1.45$) Energetic Proton Fluxes

C. High Energy Deposit Observations

The topmost channel of the REMs require over 100MeV deposited energy to count. This is equivalent to $\sim 5\text{pC}$ generated charge or $\sim 1.2 \text{ MeV}\cdot\text{cm}^2/\text{mg}$ perpendicular LET. This channel counts heavy ions and nuclear interactions from protons (proton ionisation cannot exceed the channel threshold). Figure 9 shows the count rate in this channel for both *STRV* and *Mir*, for various periods. The *STRV* data are particularly clean and show the “bump” in the inner belt due to proton nuclear reactions and a gentle rise with L -value as the geomagnetic shielding of cosmic rays is reduced. The *Mir* data are much more noisy, but a similar trend is seen. There is less obvious “bump” from the protons in the SAA. The asymptotic value is lower than *STRV* and may be due to earth “shadowing” and spacecraft shielding effects. Vertical cutoff rigidity is a function of L alone. The lowest panel shows predictions using the CREME code for *STRV* conditions. The agreement despite simplifications in shielding, large sensitive volume (slowing particles), etc., is surprisingly good.

